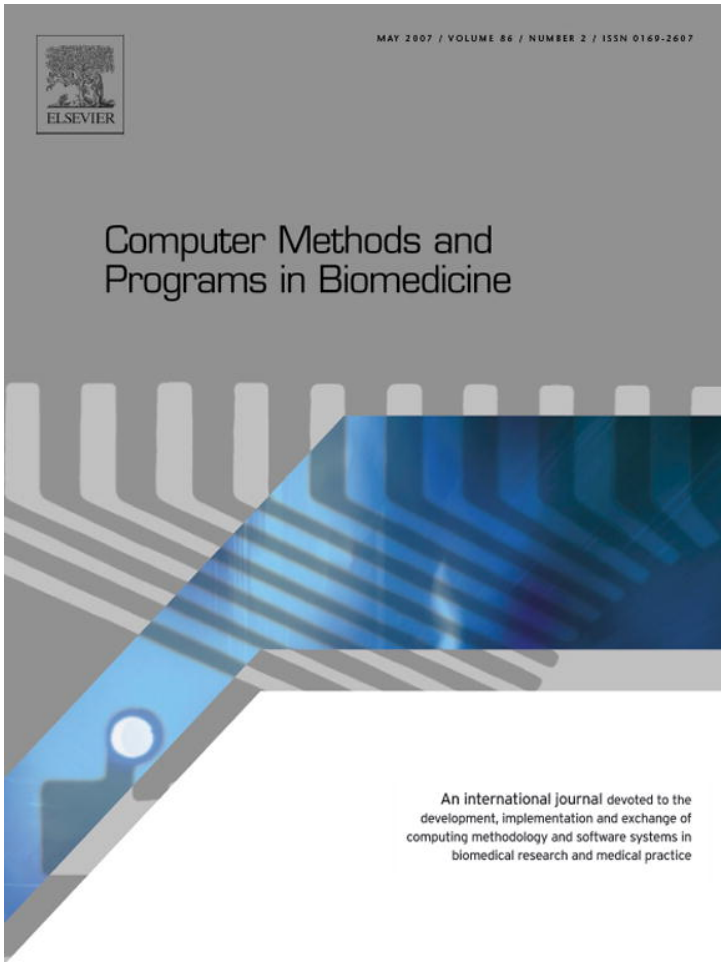

journal homepage: www.intl.elsevierhealth.com/journals/cmpb

Multi-time-scale heat transfer modeling of turbid tissues exposed to short-pulsed irradiations

*Kyunghan Kim, Zhixiong Guo**

Department of Mechanical and Aerospace Engineering, Rutgers, The State University of New Jersey, Piscataway, NJ 08854, USA

ARTICLE INFO

Article history:
Received 24 July 2006
Received in revised form
18 January 2007
Accepted 22 January 2007

Keywords:
Multiple time scales
Heat transfer
Short-pulsed lasers
Biological tissues
Computer methods

ABSTRACT

A combined hyperbolic radiation and conduction heat transfer model is developed to simulate multi-time-scale heat transfer in turbid tissues exposed to short-pulsed irradiations. An initial temperature response of a tissue to an ultrashort pulse irradiation is analyzed by the volume-average method in combination with the transient discrete ordinates method for modeling the ultrafast radiation heat transfer. This response is found to reach pseudo steady state within 1 ns for the considered tissues. The single pulse result is then utilized to obtain the temperature response to pulse train irradiation at the microsecond/millisecond time scales. After that, the temperature field is predicted by the hyperbolic heat conduction model which is solved by the MacCormack's scheme with error terms correction. Finally, the hyperbolic conduction is compared with the traditional parabolic heat diffusion model. It is found that the maximum local temperatures are larger in the hyperbolic prediction than the parabolic prediction. In the modeled dermis tissue, a 7% non-dimensional temperature increase is found. After about 10 thermal relaxation times, thermal waves fade away and the predictions between the hyperbolic and parabolic models are consistent.

1. Introduction

Many of the clinical procedures with lasers use the so-called non-ablative thermal mode of laser-tissue interaction [1,2]; that is, tissue is heated and irreversibly damaged by absorption of the laser energy. The degree and extent of tissue thermal damage depends on the rate of heat generation and transfer. Knowledge of bio-heat transfer is then very important in laser therapeutic applications.

Short-pulsed irradiation is accompanied with the use of pulsed lasers with pulse duration in the micro/nanosecond time scale. Short-pulsed lasers can be used in a wide spectrum of emerging biomedical technologies such as in laser surgery and treatment [1–4], optical imaging and diagnostics [5–7], etc. Fundamentals to these applications are knowledge of multi-time-scale heat transfer in biological tissues which includes ultrafast laser radiation transport in the micro/nano time scale and transient bio-heat transfer in the sec/min meso-time scale.

To analyze thermal response of a laser irradiated tissue and to avoid thermal damage to surrounding healthy tissue, combined thermal radiation and bio-heat modes must be considered. In the present study, we investigate the thermal response of biological tissues to short-pulsed irradiation and the importance of hyperbolic heat conduction in the prediction of accurate temperature distribution and development in the turbid tissue.

2. Background

The concept of ultrafast radiation heat transfer [8–10] was introduced to differentiate the time-dependent radiation heat transfer associated with radiation propagation in the speed

* *Corresponding author*. Tel.: +1 732 445 2024; fax: +1 732 445 3124.
E-mail address: guo@jove.rutgers.edu (Z. Guo).
0169-2607/$ – see front matter © 2007 Elsevier Ireland Ltd. All rights reserved.
doi:10.1016/j.cmpb.2007.01.009

of light (i.e., the governing equation of radiation transfer is time-dependent) from the traditional transient radiation heat transfer in which the effect of time-dependent radiation propagation is negligible (i.e., the governing equation is still stationary) and only the boundary conditions are time-dependent. Ultrafast radiation heat transfer is significant when the pulsed irradiation time is not considerably longer than the characteristic radiation propagation time in the medium. In modern technological applications, it is often accompanied with the use of short-pulsed lasers. An excellent review by Kumar and Mitra [8] has summarized the applicability and techniques for solving one-dimensional (1-D) ultrafast radiation heat transfer problems. Guo and co-workers [9–14] considered the modeling of 2-D and 3-D ultrafast radiation heat transfer and applications.

A recent review [15] compared several bio-heat models for thermal prediction in perfused tissues and concluded that the best practical approach for modeling bio-heat transfer during hyperthermia may still be the Pennes model. For irradiation times less than 5 s, the influence of blood perfusion plays a minor role and is negligible [16]; thus, the Pennes bio-heat model recedes into the heat conduction theory.

The traditional Fourier heat conduction is described by a parabolic diffusion equation which has an infinite speed of thermal propagation, indicating that a local change of temperature and/or heat generation causes an instantaneous perturbation in the temperature field. For a physical process occurring in a time interval shorter than that required for attaining thermal equilibrium, however, it has been noticed that heat wave theory [17–19] is more appropriate. The thermal wave postulate based on damped wave models leads to hyperbolic heat conduction equations and suggests a finite speed of thermal propagation. Recently Vedavarz et al. [18] examined the range of parameters over which this hyperbolic non-Fourier formulation is significant. They analyzed the thermal relaxation time for biological tissues and obtained a range of 1–100 s at room temperature. Mitra et al. [19] experimentally measured the thermal relaxation time for processed bologna meat to be 15.5 ± 2.1 s. Such large thermal relaxation times reported for biological tissues make the thermal wave theory specifically significant in the thermal modeling of pulsed laser-tissue interactions.

Many studies in the literature have considered mathematical and numerical techniques to a variety of problems via hyperbolic wave models [17–22]. The hyperbolic heat conduction involves the wave nature of thermal transport. Difficulties encountered in the numerical solution of such problems include, among others, numerical oscillations and the representation of sharp discontinuities with good resolution at the wave front. Glass et al. [20] considered the solution of one-dimensional hyperbolic conduction problems using MacCormack's scheme to handle discontinuities at the wave front with high resolution and little oscillation.

Since the speed of thermal wave propagation in biological tissues is several orders of magnitude slower than that of light, the coupling of radiative-conductive heat transfer involves two distinct time scales. Here we propose a three-step approach. First, short-pulsed radiation is absorbed in the tissue and it results in an immediate local temperature rise in the nanosecond time scale. Since the incident laser beam is axisymmetric and of Gaussian profile, the tissue is modeled as a two-dimensional axisymmetric cylinder. The ultrafast radiation heat transfer in the tissue is modeled using the transient discrete ordinates method (TDOM) developed by the authors [9]. For pulse train irradiation in microsecond/millisecond time scales, the temperature response is only a simple accumulation of single pulses. Second, thermal wave propagation starts following the local temperature rise; and the hyperbolic heat conduction is considered in the meso-time scale. The hyperbolic heat conduction equations are solved by the finite difference method using MacCormack's predictor-corrector scheme with error terms correction. Finally, thermal waves fade away and parabolic heat diffusion predominates after several thermal relaxation times. Since the last step has been extensively studied in traditional bio-heat modeling, the current study focuses on the first two steps and the comparisons with the parabolic diffusion modeling.

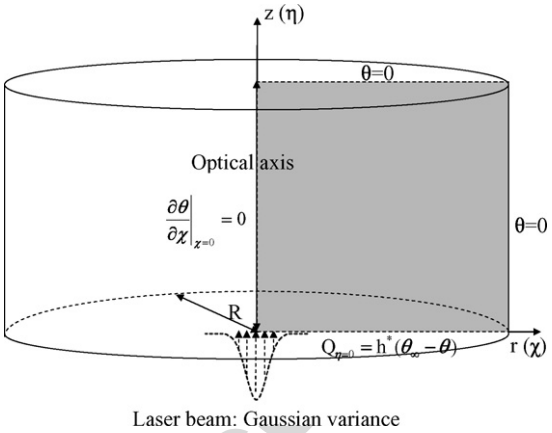

Fig. 1 – Geometric sketch of a tissue cylinder.

3. Mathematical models

The pulses of a collimated laser beam are incident into a tissue surface as shown in Fig. 1. The pulsed laser radiation heat transfer can be formulated by the transient radiative transfer equation in the cylindrical coordinates system as [9]:

$$\frac{1}{c}\frac{\partial I^l}{\partial t} + \frac{\mu_1^l}{r}\frac{\partial}{\partial r}[rI^l] - \frac{1}{r}\frac{\partial}{\partial \phi}[\mu_2^l I^l] + \mu_3^l\frac{\partial I^l}{\partial z} + (\sigma_a + \sigma_s)I^l = (\sigma_a + \sigma_s)S^l,$$
$$l = 1, 2, \ldots n, \quad (1)$$

where c is the speed of light in the medium, μ_1^l, μ_2^l and μ_3^l represent the directional cosines of a discrete ordinate direction, I^l is the directional radiation intensity, σ_a is the absorption coefficient, σ_s is the scattering coefficient, and S^l is the source term that can be expressed as:

$$S^l = (1-\omega)I_b + \frac{\omega}{4\pi}\sum_{i=1}^{n} w^i \Phi(\hat{s}^i \to \hat{s}^l) I^i + \omega S_c^l, \quad l = 1, 2, \ldots n, \quad (2)$$

where the scattering albedo $\omega = \sigma_s/(\sigma_a + \sigma_s)$ is introduced and I_b is the blackbody radiation intensity. A quadrature set of n discrete ordinates with the appropriate angular weight w is

used. The collimated laser source S_c^l in Eq. (2) is expressed by:

$$S_c^l = \frac{1}{4\pi} I_c \Phi(\hat{s}^c \to \hat{s}^l), \tag{3}$$

where the unit vector, $\hat{s}^c$, represents the collimated laser incident direction. When the reduced scattering coefficient, $\sigma_s' = (1-g)\sigma_s$, is used, the scattering phase function Φ is a unity. Here, g is the asymmetry factor.

The incident laser has a Gaussian profile both temporally and spatially. For normally incident irradiation, the beam intensity is specified as:

$$I_c(r,z,t) = (1-R)q_0 \exp\left\{-4\ln 2 \times \left[(t-z/c)/t_p - 1.5\right]^2\right\} \times \exp\left(\frac{-r^2}{v^2}\right) \times \exp(-\sigma_e z), \tag{4}$$

in which, q_0 is the amplitude of the pulse heat flux, v is the Gaussian variance, t_p is the pulse width, R is the reflectance on the tissue surface, $\sigma_e = \sigma_a + \sigma_s'$ is the reduced extinction coefficient. Here, we consider an impinging area within $0 \le r \le 2v$ and a pulse irradiation within $0 \le t \le 3t_p$. Then, the averaged incident laser power density (or fluence rate) is obtained by

$$P = \frac{N}{t_r} \cdot \frac{1}{(2v)^2} \int_0^{2v} 2r \int_0^{3p} \frac{I_c(r, z=0, t)}{1-R} dt dr = 0.2611 \frac{q_0 N t_p}{t_r}, \tag{5}$$

where N is the number of pulses and t_r is the time duration of the whole irradiation. The use of a pulse train is to avoid direct laser ablation due to extremely high flux in a short pulse.

Once the radiative intensity field is obtained, the incident radiation, and the radiative heat flux divergence can be calculated as:

$$G = \sum_{l=1}^{n} w^l I^l + I_c, \tag{6}$$

$$\nabla \cdot \mathbf{q}_{rad} = \sigma_a (4\pi I_b - G). \tag{7}$$

The local temperature response is governed by the following energy equation:

$$\rho C_p \frac{\partial T(r,z,t)}{\partial t} = -\nabla \cdot [\mathbf{q}_{cond}(r,z,t) + \mathbf{q}_{rad}(r,z,t)], \tag{8}$$

where ρ is the density, C_p is the specific heat, and T is the temperature. In hyperbolic thermal wave theory, the conductive heat flux vector is expressed by [17]

$$\tau \frac{\partial \mathbf{q}_{cond}(r,z,t)}{\partial t} + \mathbf{q}_{cond}(r,z,t) = -k\nabla T(r,z,t), \tag{9}$$

where the thermal relaxation time τ and thermal conductivity k are introduced. Introducing the thermal diffusivity $\alpha = k/\rho C_p$, the speed of thermal wave is

$$c_t = \sqrt{\frac{\alpha}{\tau}}. \tag{10}$$

When $\tau \to 0$, $c_t \to \infty$; Eq. (9) regresses to the traditional Fourier expression.

In the case of $t_p \ll \tau$, a dimensional analysis of Eqs. (8) and (9) reveals that within the short pulse duration neither thermal wave nor heat diffusion is important and the incident pulse will result in a very localized temperature response that can be described by

$$\rho C_p \frac{\partial T(r,z,t)}{\partial t} = -\nabla . \mathbf{q}_{rad}(r,z,t). \tag{11}$$

In the meso-time scale after the turning-off of the short irradiation, the energy equation in the axisymmetric cylindrical coordinates system is simplified as

$$\rho C_p \frac{\partial T(r,z,t)}{\partial t} = -\left(\frac{\partial q_{cond,r}(r,z,t)}{\partial r} + \frac{q_{cond,r}(r,z,t)}{r} + \frac{\partial q_{cond,z}(r,z,t)}{\partial z}\right). \tag{12}$$

For the sake of analysis, the hyperbolic conduction equations are converted to vector form with non-dimensional variables as follows:

$$\frac{\partial \mathbf{E}}{\partial \xi} + \frac{\partial \mathbf{F}}{\partial \chi} + \frac{\partial \mathbf{G}}{\partial \eta} + \mathbf{H} = 0 \tag{13a}$$

where

$$\mathbf{E} = \begin{bmatrix} \theta \\ Q_\chi \\ Q_\eta \end{bmatrix}, \mathbf{F} = \begin{bmatrix} Q_\chi \\ \theta \\ 0 \end{bmatrix}, \mathbf{G} = \begin{bmatrix} Q_\eta \\ 0 \\ \theta \end{bmatrix}, \mathbf{H} = \begin{bmatrix} Q_\chi/\chi \\ Q_\chi \\ Q_\eta \end{bmatrix}, \tag{13b}$$

and the non-dimensional variables are defined as:

$$\chi = \frac{r}{\sqrt{\alpha\tau}}, \quad \eta = \frac{z}{\sqrt{\alpha\tau}}, \quad \xi = \frac{t}{\tau}, \quad Q_\chi = \frac{q_{cond,r}\sqrt{\alpha\tau}}{k(T_{ref} - T_i)}, \quad Q_\eta = \frac{q_{cond,z}\sqrt{\alpha\tau}}{k(T_{ref} - T_i)}, \quad \theta = \frac{T - T_i}{T_{ref} - T_i} \tag{14}$$

In which T_i and T_{ref} are the tissue initial and reference temperatures, respectively. The reference temperature that represents the desirable temperature response induced by the irradiation is 65 °C in the present calculations. This quantity was reported as a proper temperature in laser-tissue welding to achieve optimum welding strength [3].

The tissue is assumed to be at a constant and uniform temperature of 37 °C initially. Except for the laser incident surface which is exposed to the ambient air at room temperature of 25 °C, all other surfaces of the tissue cylinder are surrounded with tissue; and thus, remained at the constant temperature. Thus, the initial and boundary conditions for the hyperbolic heat conduction model are given as

$$\theta = Q_\chi = Q_\eta = 0, \quad \text{for } \xi = 0. \tag{15a}$$

$$\frac{\partial \theta(\chi,\eta,\xi)}{\partial \chi} = 0, \quad \text{at } \chi = 0. \tag{15b}$$

$$Q_\eta = h^*(\theta_\infty - \theta), \quad \text{at } \eta = 0. \tag{15c}$$

$$\theta = 0, \quad \text{at } \chi = \chi_{max} \text{ or } \eta = \eta_{max}. \tag{15d}$$

where θ_∞ the non-dimensional ambient temperature, $h^* = \sqrt{\alpha\tau}\,h/k$, and h is the convective heat transfer coefficient.

For the radiative heat transfer analysis, Snell's law and Fresnel's law [2] are adopted at the air-tissue interface because of the mismatch of refractive indices between the two media. For the normally incident laser radiation, the reflectance on the incident surface is

$$R = \left(\frac{n-1}{n+1}\right)^2, \tag{16}$$

where n is the refractive index of the tissue. For internal radiation at the tissue–air interface, total reflection occurs when the incident angle θ_i is not less than the critical angle, $\theta_{cr} = \sin^{-1}(1/n)$, because the refractive index of a biological tissue is greater than that of air. When $\theta_i < \theta_{cr}$, the reflection on the interface is purely specular and the reflectance is calculated by Fresnel's equation:

$$R^s = \frac{1}{2}\left[\frac{\tan^2(\theta_i-\theta_r)}{\tan^2(\theta_i+\theta_r)} + \frac{\sin^2(\theta_i-\theta_r)}{\sin^2(\theta_i+\theta_r)}\right], \tag{17}$$

where θ_r is the refraction angle predicted using Snell's law.

Since biologic tissues are generally highly scattering, photons reaching the other boundaries of the tissue cylinder have been undergone multiple scattering events and the possibilities of photons passing through the boundary or reflecting back are almost equal. Thus, we specify a diffuse reflectance of 0.5 on such surfaces. The reflecting boundary conditions can be represented by [12,13]

$$I_w^l = R^s I_w^{-l} + \frac{R^d}{\pi}\left[I_{cw} + \sum_{\hat{n}\cdot\hat{s}^j<0} w^j I_w^j \left|\hat{n}\cdot\hat{s}^j\right|\right]. \tag{18}$$

In the present models the following assumptions are adopted:

(1) The volume-average method is used for predicting local temperature response during a short irradiation period. Since the thermal wave speed in tissues is generally in the order of 10^{-4} mm/ms, the propagation of a thermal wave is 10^{-4} mm in 1 ms. As compared with the dimension of a turbid tissue (1–100 mm), thermal propagation and diffusion are negligible within 1 ms.
(2) Tissue radiation emission is neglected because the tissue blackbody intensity is much smaller than the incident laser intensity.
(3) Tissue optical and thermal properties are thermally stable during the heat transfer process.
(4) Blood perfusion and thermal evaporation and/or phase change of tissue during the heat transfer process are not considered.

The considered human tissues include dermis, aorta, heart (endocardium), and uterus. The optical properties of these tissues are listed in Table 1, in which the data are cited from Cheong et al. [23]. It is seen that the tissue absorption is generally much weaker than the scattering. The tissue density and specific heat are chosen in 70% water tissue condition such that $\rho C_p = 3.52 \times 10^6$ (J/m^{3}K) [24]. The thermal diffusivity is assumed to be 0.14×10^{-6} m^2/s [25]. The thermal relaxation time for thermal wave propagation is assumed to be 16 s [18,19]. The above thermal property values are assumed for all the four considered human tissues in spite of the fact that small variations in thermophysical properties exist among different soft tissues and/or individuals. The non-dimensional radius and thickness of the tissue cylinders are selected as 10 to minimize the tissue boundary effect and wave echo. The non-dimensional Gaussian variance of the incident laser beam is 0.65. The heat transfer coefficient at the tissue/air interface is assumed to be 15 W/(m^{2}K).

Table 1 – The optical properties of human tissues (data are cited from [23]).

Tissue type	Optical properties	
	σ_a (mm^{-1})	σ_s'(mm^{-1})
Dermis	0.27	3.55
Aorta	0.052	4.1
Heart (endocardium)	0.007	0.367
Uterus	0.035	12.214

4. Numerical schemes

The TDOM with S_{10} scheme was employed for the solution of the present ultrafast radiation heat transfer problem. For information on the numerical scheme and accuracy validation, please refer to our recent publication [9] for the cylindrical coordinates system or to Guo and Kumar's publications [12,13] for the Cartesian coordinates system. Therefore, the details of the numerical method on radiative transfer are not repeated here.

To solve the hyperbolic heat conduction equations, MacCormack's predictor-corrector scheme is adopted. The scheme has been known to deal with thermal wave propagation very well in 1-D problems [20,21]. Here it is extended to 2-D axisymmetric cylindrical problems. The discretized forms of the non-dimensional hyperbolic conduction equations are as follows:

Predictor:

$$\tilde{\mathbf{E}}_{i,j}^{n+1} = \mathbf{E}_{i,j}^n - \nu_x(\mathbf{F}_{i+1,j}^n - \mathbf{F}_{i,j}^n) - \nu_y(\mathbf{G}_{i,j+1}^n - \mathbf{G}_{i,j}^n) - \Delta\xi\mathbf{H}_{i,j}^n \tag{19a}$$

Corrector:

$$\mathbf{E}_{i,j}^{n+1} = \frac{1}{2}[\mathbf{E}_{i,j}^n + \tilde{\mathbf{E}}_{i,j}^{n+1} - \nu_x(\tilde{\mathbf{F}}_{i,j}^{n+1} - \tilde{\mathbf{F}}_{i-1,j}^{n+1}) - \nu_y(\tilde{\mathbf{G}}_{i,j}^{n+1} - \tilde{\mathbf{G}}_{i,j-1}^{n+1}) - \Delta\xi\tilde{\mathbf{H}}_{i,j}^{n+1}]. \tag{19b}$$

von Neumann stability analysis was conducted and the stability criterion is:

$$\nu_x^2 + \nu_y^2 \le 1 \tag{20}$$

The two Courant numbers are defined as $\nu_x = \Delta\xi/\Delta\chi$ and $\nu_y = \Delta\xi/\Delta\eta$.

MacCormack's scheme is explicit and has second-order accuracy. The modified equation is determined as

$$\frac{\partial \mathbf{E}}{\partial \xi} + \frac{\partial \mathbf{F}}{\partial \chi} + \frac{\partial \mathbf{G}}{\partial \eta} + \mathbf{H} + \frac{\partial}{\partial \chi}(\Delta_2 \mathbf{F} + \Delta_3 \mathbf{F}) + \frac{\partial}{\partial \eta}(\Delta_2 \mathbf{G} + \Delta_3 \mathbf{G}) + O(\Delta^4) = 0, \tag{21a}$$

where the error terms are

$$\Delta_2 \mathbf{F} = \frac{1}{3!}(\Delta\chi)^2 \left[(1-\nu_x^2)\frac{\partial^2 \mathbf{F}}{\partial \chi^2}\right], \quad \Delta_2 \mathbf{G} = \frac{1}{3!}(\Delta\eta)^2 \left[(1-\nu_y^2)\frac{\partial^2 \mathbf{G}}{\partial \eta^2}\right], \tag{21b}$$

$$\Delta_3 \mathbf{F} = \frac{1}{4!}(\Delta\chi)^3 \left[3\nu_x(1-\nu_x^2)\frac{\partial^3 \mathbf{F}}{\partial \chi^3}\right],$$

$$\Delta_3 \mathbf{G} = \frac{1}{4!}(\Delta\eta)^3 \left[3\nu_y(1-\nu_y^2)\frac{\partial^3 \mathbf{G}}{\partial \eta^3}\right]. \tag{21c}$$

Because of the stability constrain, the Courant numbers cannot be unity. Thus, the error terms in Eq. (21) exist and correction of the error terms in Eq. (13) is important because it is the modified equation that is actually solved when Eq. (13) is integrated by MacCormack's scheme. This can be done by subtracting the error terms from Eq. (13), which then becomes

$$\frac{\partial \mathbf{E}}{\partial \xi} + \frac{\partial \mathbf{F}_0}{\partial \chi} + \frac{\partial \mathbf{G}_0}{\partial \eta} + \mathbf{H} = 0, \tag{22a}$$

where

$$\mathbf{F}_0 = \mathbf{F} - \Delta_2 \mathbf{F} - \Delta_3 \mathbf{F}, \tag{22b}$$

$$\mathbf{G}_0 = \mathbf{G} - \Delta_2 \mathbf{G} - \Delta_3 \mathbf{G}. \tag{22c}$$

When MacCormack's method is applied to Eq. (22), the resulting modified equation does not contain the second-order and third-order error terms. In the present computations, the error terms are discretized by second-order accurate approximations.

For both the radiation and hyperbolic conduction simulations, the same grid system is adopted to avoid interpolation. The radius of the tissue cylinder is equal to its thickness so that the cylinder is meshed by 100 × 100, or 200 × 200, or 300 × 300 grids in the $r - z$ ($\chi - \eta$) plane. In such situations, the Courant numbers in the radial and axial directions are equal. The simulation results for the three sets of grids were consistent and the difference between the 200^2 and 300^2 grids were generally within 2%. Thus, the results for the tissue cylinders presented in the next section are from the 200 × 200 grid system. For the

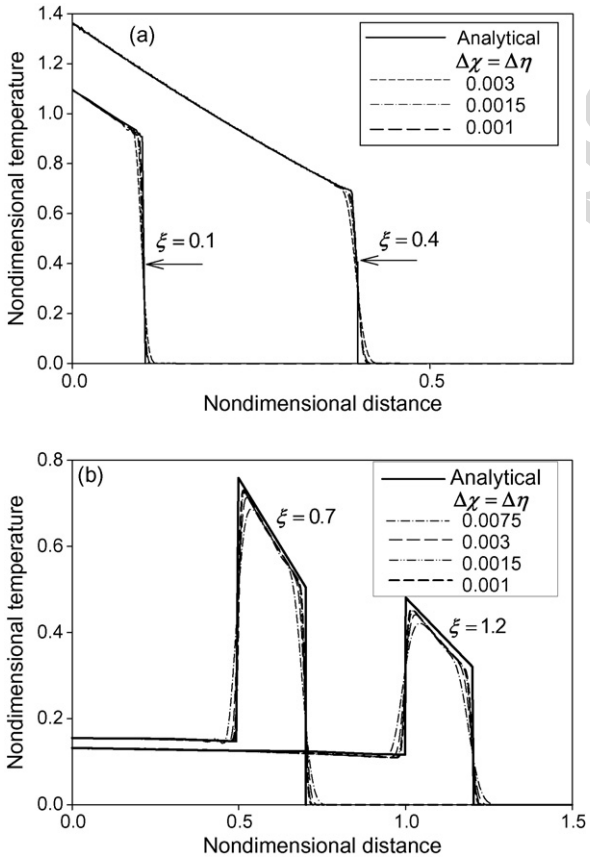

Fig. 2 – Comparisons of the numerical results with the analytical solutions [22] of the temperature profiles along the cylinder centerline: (a) continuous source; and (b) single pulse source.

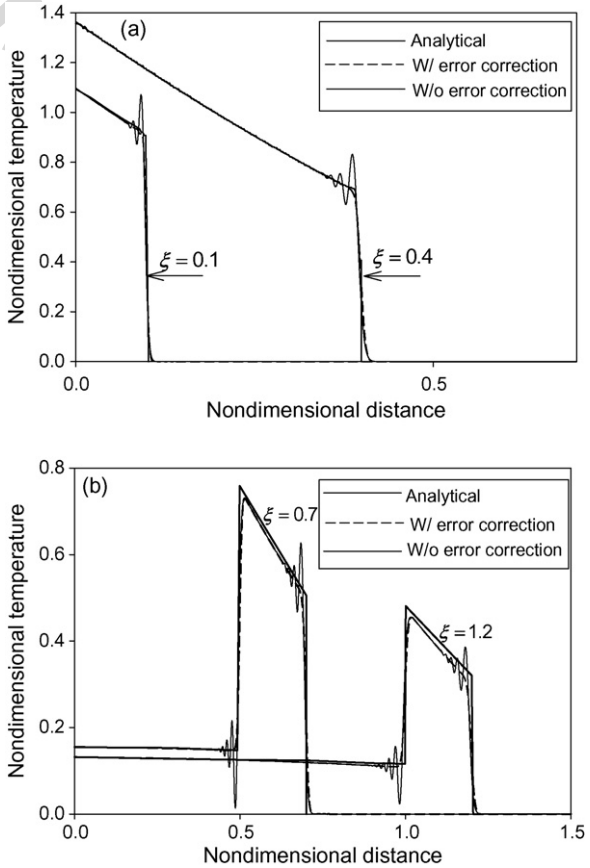

Fig. 3 – Comparisons of the calculated temperature profiles along the cylinder centerline with and without error terms correction: (a) continuous source; and (b) single pulse source.

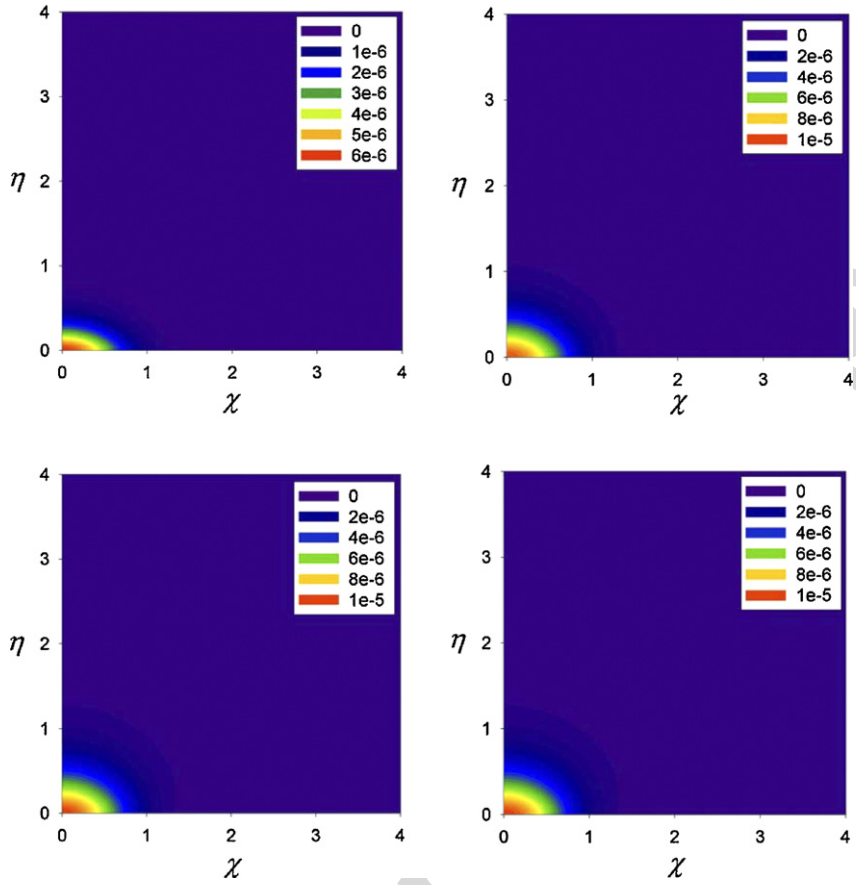

Fig. 4 – Contours of the non-dimensional temperature fields of the dermis tissue subject to an ultrashort pulse irradiation at selected time instants: at (a) t = 20 ps; (b) t = 40 ps; (c) t = 100 ps; and (d) t = 500 ps.

hyperbolic conduction modeling, the non-dimensional time step $\Delta\xi$ is generally selected to be half of the non-dimensional spatial grid size. Thus, the Courant number in both directions is 0.50 and the computations are stable. Actually we tested three different Courant numbers, i.e., 0.2, 0.5, and 0.7. For MacCormack's scheme without the error terms correction, a small Courant number (0.2) tends toward strong numerical oscillation. When the error terms are corrected, however, numerical oscillations vanish for all the three considered Courant numbers.

For the ultrafast radiation heat transfer modeling, we consider a pulse width of 10 ps. The time step is 0.2 ps and the calculation time is extended to 1 ns such that a stable local temperature rise is achieved. The irradiation contains usually

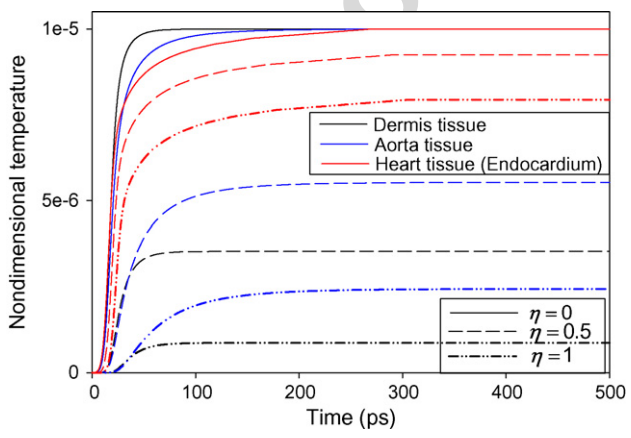

Fig. 5 – Temporal profiles of the non-dimensional temperatures at different locations in the tissues subject to an ultrashort pulse irradiation.

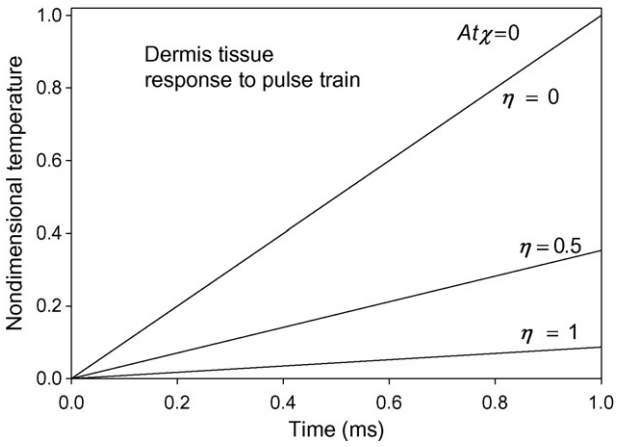

Fig. 6 – Temporal profiles of the non-dimensional temperatures in the dermis tissue exposed to 1 ms pulse train irradiation.

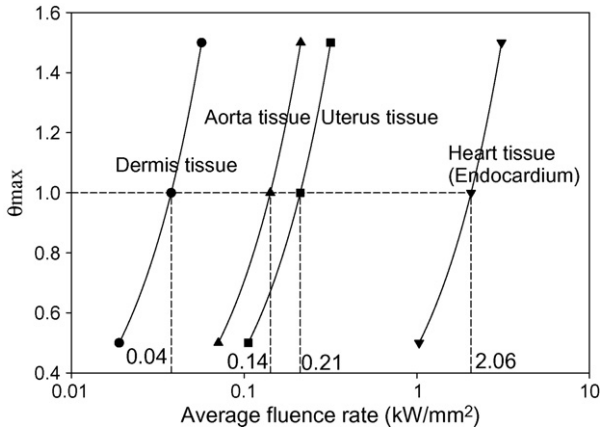

Fig. 7 – The maximum temperature at the laser spot center vs. the incident laser power for various tissues.

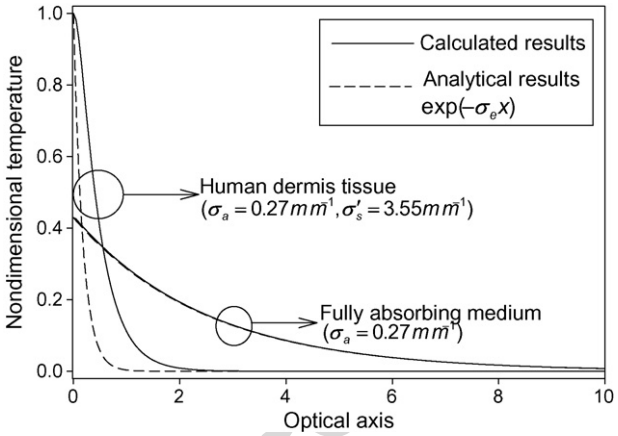

Fig. 8 – Comparisons of the non-dimensional temperature profiles along the cylinder centerline subject to 1 ms pulse train irradiation predicted by the radiative heat transfer modeling and simple Lambert-Beer's analysis, respectively.

many such short pulses. In the present calculations, 10^5 pulses are irradiated during 1 ms. After that, the irradiation is turned off for purely thermal wave or diffusion treatment.

5. Results and discussion

The current computational code is validated through comparison of numerical results with analytical solutions. Let's consider a hyperbolic heat conduction problem in a semi-infinite region due to axisymmetric continuous or pulsed surface heat sources. The problem has been described and analytically solved by Kim et al. [22]. The irradiation source is simplified as a surface heat flux. In the calculations both the non-dimensional radius and thickness of the cylinder are

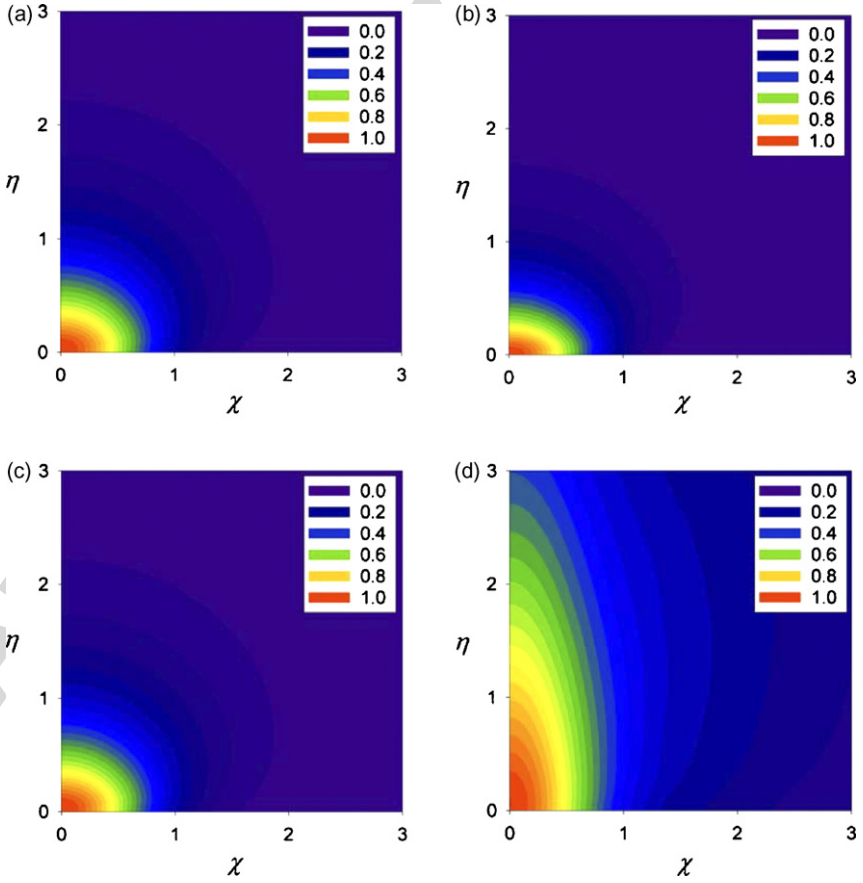

Fig. 9 – Comparisons of the non-dimensional temperature fields induced by the 1 ms pulse train radiation heat transfer: (a) dermis tissue; (b) uterus tissue; (c) aorta tissue; and (d) heart tissue.

set at 1.5. Fig. 2(a) and (b) show the comparisons of the calculations with the analytical exact solutions for the continuous and single pulse sources, respectively. The non-dimensional temperature profiles along the cylinder centerline at different time instants are selected for comparison. Various grid sizes are considered in the calculations with a constant Courant number of 0.5. It is seen that the numerical results for the case with a continuous source match excellently with the exact solutions. The sharp wave fronts are well captured. The numerical results for the case with a single pulse source generally match with the exact solutions. The grid size influences the quality of the simulated wave fronts in Fig. 2(b). With coarse grid sizes the dissipative effect is obvious and the gradients at the wave fronts tilt. With refining grid sizes the sharp wave fronts are well captured. However, it is worthy of mentioning that the refining of grid system will increase computer memory and CPU time; and there is always a compromise between accuracy and computation costs.

Fig. 3 demonstrates the importance of the error terms correction in MacCormack's scheme using the above exemplary problem. The grid size is $\Delta\chi = \Delta\eta = 0.001$ and the Courant number is still 0.5. Strong numerical oscillations at the wave fronts are observed in the numerical results without correction of the error terms. These oscillations are due to the dominance of the odd derivate error terms over the even derivate term. However, the numerical oscillations are eliminated when the error terms are corrected.

Now let's consider transient heat radiation and conduction problems in turbid tissues exposed to short-pulsed irradiation. Fig. 4 shows the contours of the temperature fields in the dermis tissue subject to a 10 ps pulse at four different time instants. At $t = 20$ ps, the temperature field is confined in a superficial regime around the laser spot. At $t = 40$ ps, the temperature field is penetrated axially due to radiation propagation. Also the magnitude of temperature at $t = 40$ ps is greater than that at $t = 20$ ps, because of the continuous absorption of the Gaussian irradiation (up to $3t_p$). The temperature fields at $t = 100$ and 500 ps are further enlarged as compared with the figure at $t = 40$ ps. However, the expansion speed of the temperature field gradually slows down. This is because the local temperature response depends on the local volume-average accumulation of radiation energy absorption. When the incident pulse is turned off after $3t_p$, the source for radiation absorption comes only from the scattered radiation. As time elapses, the scattered radiation becomes weaker and weaker.

Fig. 5 shows the temperature responses of three tissue types to a single 10 ps pulse at three selected positions in the centerline ($\chi = 0$; $\eta = 0$, 0.5, and 1). It is seen that, at the location of $\eta = 1$ the temperature in the heart tissue is much higher than the temperatures in the aorta and dermis tissues. The large absorption of the dermis tissue will confine the laser radiation in a small area. When the changes of the temporal temperatures at all locations become very flat, pseudo steady state of the temperature response is then reached. The time for achieving the pseudo steady state responding to a single short pulse depends mainly on the tissue properties. It is found that longer time is required for weakly absorbing tissues, such as the heart tissue. Generally the temperature field will reach to pseudo steady state condition in 1 ns for all the considered tissues.

The pulse train response in the microsecond/millisecond time scales with negligible thermal wave and diffusion is then a simple addition of the pseudo steady state temperature of the single pulses. In Fig. 6, the temporal temperature responses of the dermis tissue subject to pulse train irradiation (10^5 short pulses within 1 ms) are plotted at three selective positions. The responses are linear at all positions unless they

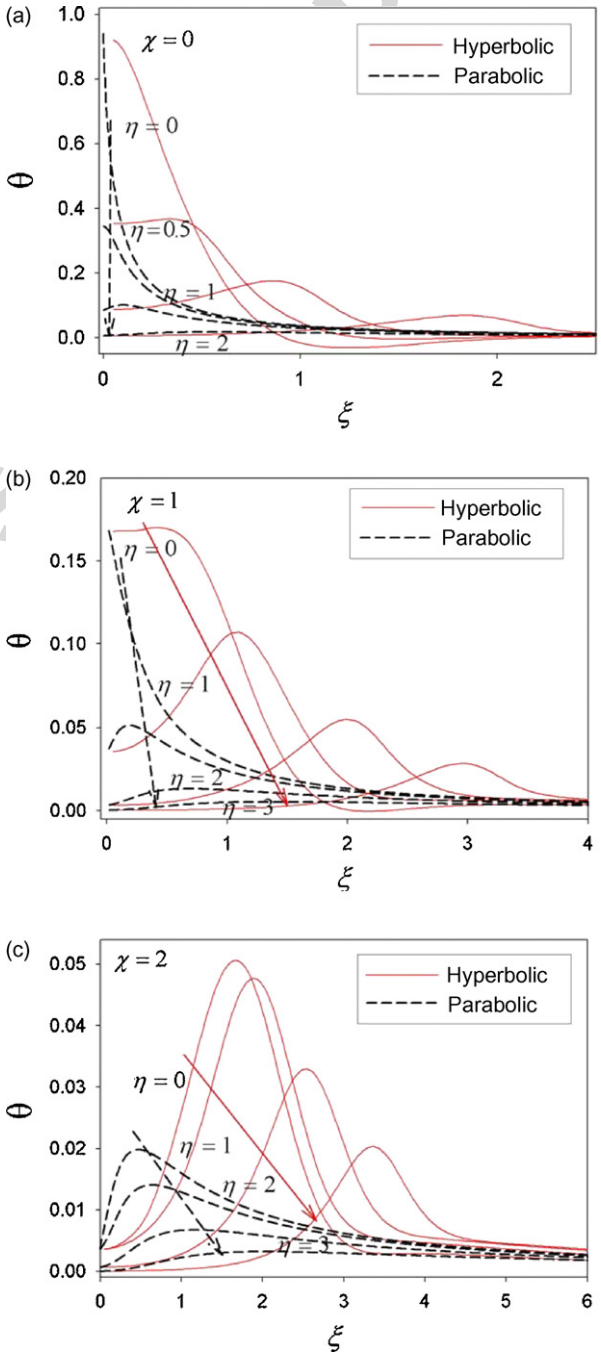

Fig. 10 – Comparisons of the temporal profiles of the non-dimensional temperature in the dermis tissue between the hyperbolic conduction and parabolic diffusion predictions.

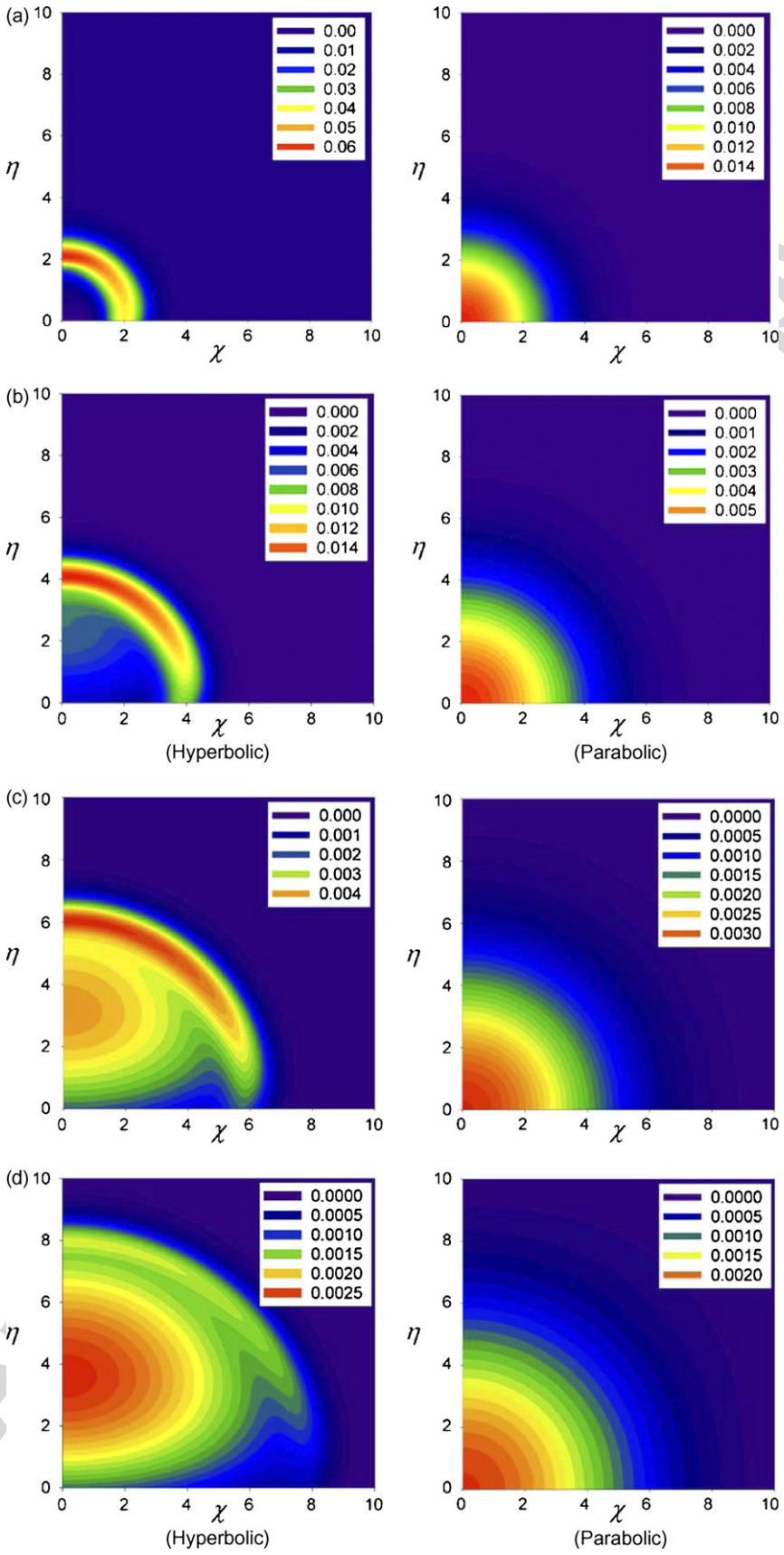

Fig. 11 – Comparisons of the non-dimensional temperature fields in the dermis tissue between hyperbolic conduction and parabolic diffusion models at four different meso-time instants: (a) $\xi = 2$;(b) $\xi = 4$;(c) $\xi = 6$; and (d) $\xi = 8$.

are inspected in the picosecond/nanosecond time scales as shown in Fig. 5. In the following figures, the irradiation condition is assumed to be a pulse train of 10^5 pulses in 1 ms.

In the present studies, the incident laser power is adjusted to let the maximum temperature at the laser spot be a unity. Fig. 7 shows the relationships between the maximum temperature at the laser spot center and the laser power density with pulse train irradiation for the four tissues. The smaller the tissue absorption coefficient, the higher is the required laser power. Thus, increasing tissue absorption in the target area is important in laser surgery and treatment applications. This can be realized through proper selection of laser wavelength [1], use of endogenous or exogenous chromophores [3,9], etc. It should be mentioned that relationships are linear when tissue emission is neglected. A logarithmic scale is used in the abscissa in Fig. 7.

Fig. 8 shows the spatial variance of the non-dimensional temperature along the dermis tissue cylinder centerline at time instant of 1 ms, where the calculated results are compared with the simple Lambert-Beer's analyses. This temperature profile is determined by the local radiation deposition through radiation heat transfer analysis. When scattering is neglected, the numerical result for the fully absorbing medium matches excellently with the Lambert-Beer's analysis. Since scattering in the dermis tissue is strong, the analytical result from simple Lambert-Beer's law does not match with the simulation. For absorbing-scattering tissues, therefore, Lambert-Beer's law may not be a good approximation. Instead accurate radiation heat transfer modeling is desirable.

The immediate temperature fields induced purely by radiation absorption of the pulse train are compared in Fig. 9 between different tissue types. It is seen that the temperature patterns vary, depending on the tissue extinction coefficient. In the uterus tissue (has the largest σ_e among the four tissues), the temperature is concentrated in a very small region. In the heart tissue (has the smallest σ_e among the four tissues), the temperature field penetrates to deep tissue. The temperature fields are similar in the aorta and dermis tissues because they have similar σ_e values.

Thermal wave propagation follows the immediate local temperature rise, but it is only significant in the meso-time scale. In Fig. 10, the temporal temperature profiles in the dermis tissue at several selected locations are displayed. Strong wave behavior is observed when $0<\xi<4$ where the temperature changes periodically with decreasing amplitude. To understand the differences between the hyperbolic heat conduction and traditional Fourier parabolic heat diffusion, the results predicted by the parabolic diffusion model are also plotted in Fig. 8. The finite difference method with explicit scheme was used for the diffusion simulation. Since this technique is mature and well-described in the literature and texts, it is not repeated here. In the parabolic diffusion prediction, the temperature decays exponentially and more slowly than the hyperbolic counterpart. It is noticeable that the hyperbolic wave model predicts larger maximum temperatures at positions beyond the laser spot center than the parabolic diffusion model. When the time reaches to 10 thermal relaxation times, the thermal waves fade away and the predictions between the hyperbolic and parabolic models are consistent.

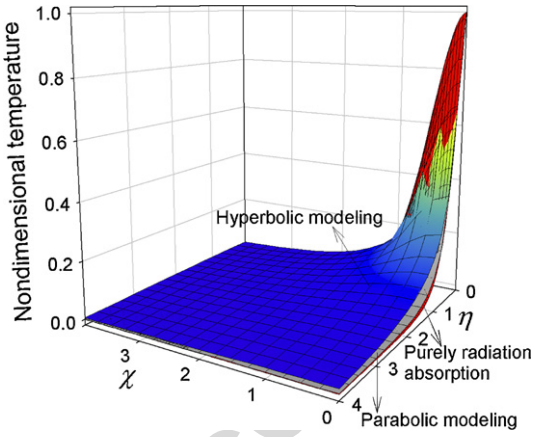

Fig. 12 – Comparisons of the maximum temperature maps in the dermis tissue due to purely radiation heat transfer or combined heat transfer predicted by the hyperbolic and parabolic models, respectively.

Fig. 11 shows the contours of the temperature fields in the dermis tissue at various time stages. The results from both the hyperbolic and parabolic models are given for comparison. In the temperature distributions predicted by the hyperbolic model, clear wave front propagation is observed. The temperatures in the wave fronts are generally high, leading to larger magnitudes in the temperature spectra in the contours of hyperbolic modeling. As time elapses, the wave front weakens and a diffusion field is quickly developing behind the front. The temperature fields predicted by the parabolic model are concentrated in the vicinity around the laser spot and a large temperature gradient exists there.

In Fig. 12, the maximum temperature maps in the dermis tissue are plotted for comparison between the hyperbolic and parabolic models, where the maximum temperature for

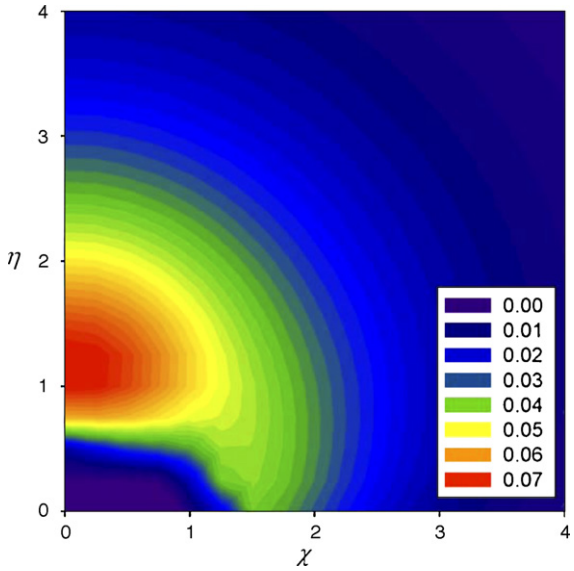

Fig. 13 – Contour of the maximum non-dimensional temperature difference in the dermis tissue between the hyperbolic and parabolic models.

each location during the entire hyperbolic or parabolic heat transfer process is selected. The maps are useful for estimating the thermal damage zone. It is found that in a small zone around the laser incident spot, the maximum temperature is determined by the direct radiation absorption. While in other regions, the hyperbolic model generally predicts larger maximum temperature than the parabolic model. Thus, its thermal damage zone is larger than that predicted by the parabolic model. This finding could be significant for many laser biomedical applications. The temperature difference between the two model predictions is further visualized in Fig. 13. A 7% non-dimensional temperature increase is observed in some region with the hyperbolic prediction.

6. Conclusion

The combined radiation and conduction heat transfer model is proposed and employed to simulate multi-time-scale heat transfer in turbid tissues subject to short-pulsed irradiation. This model integrates three steps. In the first step, ultrafast radiation heat transfer of a tissue subject to a single ultrashort pulse irradiation is modeled; and an initial local temperature response at the picosecond/nanosecond time scale is obtained. Pseudo steady state temperature response in the tissues is found within 1 ns. If the incident pulse or pulse train is in the microsecond/millisecond time scales, the temperature response is a simple accumulation of the pseudo steady state temperature for all the pulses. In the second step, thermal wave propagation is considered at the meso-time scale. In the third step, thermal waves fade away and the parabolic heat diffusion predominates.

Accurate radiation heat transfer modeling is needed in order to predict local temperature rise due to radiation absorption because biological tissues are generally highly scattering. The temperature distribution pattern of a tissue induced by direct radiation absorption depends on the absorption coefficient as well as the extinction coefficient. For the uterus tissue, high temperature is concentrated in a very small region. While for the heart tissue, high temperature penetrates to deep tissue. The temperature fields are similar in the aorta and dermis tissues because of small difference in their extinction coefficients.

The numerical method for the hyperbolic conduction model is validated in an exemplary problem through comparison with analytical solution. A good agreement between the numerical and analytical results is found. The error terms correction in the modified equation is required for eliminating the numerical oscillation. The temperatures in the dermis tissue subject to a pulse train irradiation predicted by the hyperbolic heat conduction are compared with the parabolic heat diffusion predictions. In the hyperbolic conduction modeling, temperature changes periodically with decreasing amplitude. In the parabolic conduction modeling, however, temperature rises first and then decays exponentially. After several thermal relaxation times the thermal wave behavior is substantially weakened and the predictions between the hyperbolic and parabolic models are consistent. The obtained maximum local temperature maps show that the hyperbolic model predicts a larger thermal damage zone than the parabolic model.

REFERENCES

[1] R.R. Anderson, J.A. Parrish, Selective photothermolysis: precise microsurgery by selective absorption of pulsed radiation, Science 220 (1983) 524–527.
[2] M.H. Niemz, Laser-Tissue Interactions, Springer, New York, 1996, Chap. 3.
[3] L.S. Bass, M.R. Treat, Laser tissue welding: a comprehensive review of current and future applications, Lasers Surg. Med. 17 (1995) 315–349.
[4] R.R. Anderson, Dermatological history of the ruby laser: the long story of short pulses, Arch. Dermatol. 139 (2003) 70–74.
[5] Y. Yamada, Light-tissue interactions and optical imaging in biomedicine, Annu. Rev. Heat Transfer 6 (1995) 1–59.
[6] H. Quan, Z. Guo, Fast 3-D optical imaging with transient fluorescence signals, Opt. Express 12 (2004) 449–457.
[7] Z. Guo, S.K. Wan, D.A. August, J. Ying, S.M. Dunn, J.L. Semmlow, Optical imaging of breast tumor through temporal log-slope difference mappings, Comput. Biol. Med. 36 (2006) 209–223.
[8] S. Kumar, K. Mitra, Microscale aspects of thermal radiation transport and laser applications, Adv. Heat Transfer 33 (1999) 187–294.
[9] K.H. Kim, Z. Guo, Ultrafast radiation heat transfer in laser tissue welding and soldering, Numer. Heat Transfer, Part A 46 (2004) 23–46.
[10] Z. Guo, S. Kumar, Radiation element method for transient hyperbolic radiative transfer in plane-parallel inhomogeneous media, Numer. Heat Transfer, Part B 39 (2001) 371–387.
[11] Z. Guo, S. Kumar, K.C. San, Multi-dimensional Monte Carlo simulation of short pulse laser radiation transport in scattering media, J. Thermophys. Heat Transfer 14 (2000) 504–511.
[12] Z. Guo, S. Kumar, Discrete-ordinates solution of short-pulsed laser transport in two-dimensional turbid media, Appl. Opt. 40 (2001) 3156–3163.
[13] Z. Guo, S. Kumar, Three-dimensional discrete ordinates method in transient radiative transfer, J. Thermophys. Heat Transfer 16 (2002) 289–296.
[14] Z. Guo, K.H. Kim, Ultrafast-laser-radiation transfer in heterogeneous tissues with the discrete-ordinates method, Appl. Opt. 42 (2003) 2897–2905.
[15] H. Arkin, L.X. Xu, K.R. Holmes, Recent developments in modeling heat transfer in blood perfused tissues, IEEE Trans. Biomed. Eng. 41 (1994) 97–107.
[16] A.J. Welch, E.H. Wissler, L.A. Priebe, Significance of blood flow in calculations of temperature in laser irradiated tissue, IEEE Trans. Biomed. Eng. 27 (1980) 164–166.
[17] D.D. Joseph, L. Preziosi, Heat waves, Rev. Modern Phys. 61 (1989) 41–73.
[18] A. Vedavarz, S. Kumar, M.K. Moallemi, Significance of non-fourier heat waves in conduction, J. Heat transfer 116 (1994) 221–224.
[19] K. Mitra, S. Kumar, A. Vedavarz, M. Moallemi, Experimental evidence of hyperbolic heat conduction in processed meat, J. Heat Transfer 117 (1995) 568–573.
[20] D.E. Glass, M.N. Ozisik, D.S. McRae, B. Vick, On the numerical solution of hyperbolic heat conduction, Numer. Heat Transfer 8 (1985) 497–504.
[21] D.E. Glass, M.N. Ozisik, D.S. McRae, B. Vick, Hyperbolic heat conduction with surface radiation, Int. J. Heat Mass Transfer 28 (1985) 1823–1830.

[22] W.S. Kim, L.G. Hector Jr., M.N. Ozisik, Hyperbolic heat conduction due to axisymmetric continuous or pulsed surface heat sources, J. Appl. Phys. 68 (1990) 5478–5485.
[23] W.F. Cheong, S.A. Prahl, A.J. Welch, A review of the optical properties of biological tissues, IEEE J. Quantum Electron 26 (1990) 2166–2185.
[24] B. Choi, A.J. Welch, Analysis of thermal relaxation during laser irradiation of tissue, Lasers Surg. Med. 29 (2001) 351–359.
[25] M.L. Cohen, Measurement of the thermal properties of human skin, A Rev. J. Invest. Dermatol. 69 (1977) 333–338.